Experimental Study of Non-Destructive Approach on PEMFC Stack Using Tri-Axis Magnetic Sensor Probe

Yutaro Akimoto, Keiichi Okajima

Graduate School of Systems and Information Engineering, University of Tsukuba, Tsukuba, Japan
Email: r1220585@risk.tsukuba.ac.jp

Abstract

In this paper, the current distribution in a 300-W-class PEMFC stack was investigated in order to determine the operating state of the stack. Measurements of the magnetic field were performed on several cells in the stack. The vector of the magnetic field expressed the direction of the macroscopic current, which was from the anode side to the cathode side. This direction matched the polarity of the stack. In the measurement results, current distributions differed among cells; each cell had a different performance. Furthermore, we have tried to evaluate faults, such as flooding, by measuring the magnetic field and variations in the voltage.

Keywords

1. Introduction

The use of fuel cells is expected to mitigate environmental problems such as exhaustion of fossil fuels and greenhouse gas emissions. One type of fuel cell, the proton-exchange membrane fuel cell (PEMFC), has low operation temperature and exhibits rapid start-up; therefore, it is used in not only co-generation systems [1] but also fuel cell vehicles (FCVs) [2]. The widespread commercialization of PEMFC stacks depends on their reliability and fault diagnosis. The requirements for PEMFC lifetime according to the US Department of Energy (DOE) are 5000 h for vehicles and 40,000 h for stationary applications. PEMFC stacks are currently unable to achieve these lifetimes [3].

Many diagnostic methods have been developed for PEMFCs. The current distribution in a stack is essential for determining the operating conditions of the stack. Conditions such as partial gas pressure, operating temper-

ature, and humidity are not uniform among different cells. Some current distribution measurement methods have been developed using the segmented cell. Cleghorn *et al.* proposed the method [4]. Ghosh *et al.* constructed the passive network in PEMFC using the segmented bipolar plates (BP) [5]. Wieser *et al.* used the Hall sensors for the method [6]. Alaefour *et al.* demonstrated the relationship between the current distributions and the operations conditions using the print circuit board (PCB), segmented BP and current collector [7] [8]. However, this method has disadvantages of complexity, cost, and inaccuracy. Further, the passive resistor network, the PCB, and the Hall sensors must be embedded in the cells, and electric contact must be established.

In order to solve these problems, non-destructive, *in-situ* approaches have been developed. Some of these methods involve visualizing water transport in PEMFCs. Water in fuel cells has been visualized using soft X-ray radiography [9] and magnetic resonance imaging [10]. However, these methods are difficult to apply to PEMFC stacks because of the bulky equipment required. The measurement of current distribution in cells using magnetic sensors investigated. Hauer *et al.* proposed the non-destructives measurement method using the magnetic sensors [11]. Izumi *et al.* have enabled the mapping of current distribution in a single cell using simple equipment [12]. Katou *et al.* expected the current distribution using the magnetic-impedance sensor and 3 dimensional inverse problem FEM [13]. Nonetheless, these methods cannot be applied to a fuel cell stack. Additionally, these studies have not clarified the relationship between current distribution and cell performance. Therefore, it is important to evaluate this relationship in a stack using the non-destructive method.

We developed the measurement of current distribution in a stack using a tri-axial magnetic sensor probe inserted into cooling holes. This method has advantages of being non-destructive and enabling non-contact measurement. In the past, the Nexa Power module 1.2-kW PEMFC stack under the steady state has been evaluated [14] [15]. In this study, current distribution was investigated to determine the operating state of a 300-W-class PEMFC stack using a new tri-axial magnetic sensor probe. Furthermore, we have tried to evaluate faults, such as flooding and the others by measuring the magnetic field and variations in voltage.

2. Experimental PEMFC Set up and Operating Conditions

All experiments were performed using an air-cooled 300-W-class PEMFC stack. The fuel cell system is shown in **Figure 1**. Hydrogen (>99.99%) was supplied to the anode without humidification at 100 kPa in a dead-end mode and purged every 10 minutes. Dry air was supplied to the cathode, and the flow rate was measured using a digital flow meter. The stack comprised 20 cells connected in series, and the cells were numbered 1 - 20 starting from the side of the hydrogen inlet. A 330-kW DC electric load (Kikusui: PLZ334W) was used for all experiments aimed at evaluating the fuel cell stack performance. The stack was operated at a constant current, and the cell voltages were measured using a data logger (HIOKI: 8422-50).

In this study, stack current I was 10 A in the steady state. The supplied air flow rates were 20, 18, 16, 14, 12, 10, and 9 L/min. The operating temperature of the fan was 35˚C. The ambient temperature was 25˚C ± 1˚C. The relative humidity was 40% ± 3%.

3. Methodology

3.1. Current Distribution Measurements

Magnetic fields were measured by inserting the magnetic sensor into the cooling holes of the stack. **Figure 2** shows a schematic diagram of the magnetic field measurement device and the picture of the magnetic sensor probe. The magnetic sensor was a tri-axis electronic compass (Aichi Micro Intelligent: AMI306). This sensor has dimensions of $2.0 \times 2.0 \times 1.0$ mm and was embedded with MI sensors. Each sensor outputs the magnetic flux density of the corresponding axis. Output values were recorded on a PC through the I2C interface.

The electric current generated by the PEMFC produces a magnetic field by the Biot-Savart law. Reference axes were set for the current distribution measurements. The *x*-axis was the cell width, the *y*-axis was the cell height, and the *z*-axis was perpendicular to the cell surface. The *x*, *y* component of magnetic flux density was corresponded the stack current by the law. Additionally, the *z* component was explained the current parallel to the surface of the cell by the fault such as flooding.

The measurement device outputs the *x*, *y*, and *z* components of the magnetic flux density: B_x, B_y, and B_z, respectively. The following *x* and *y* components of the current were used:
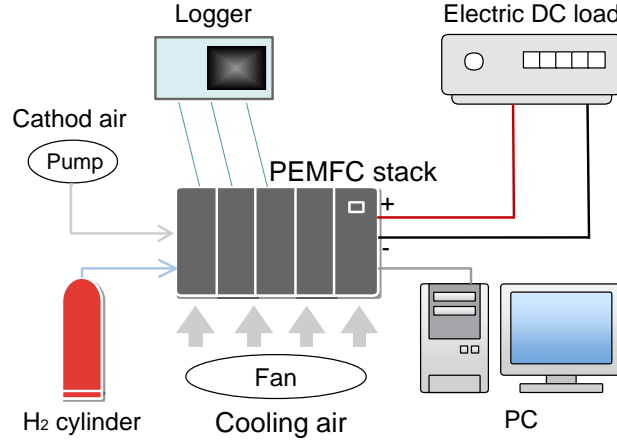
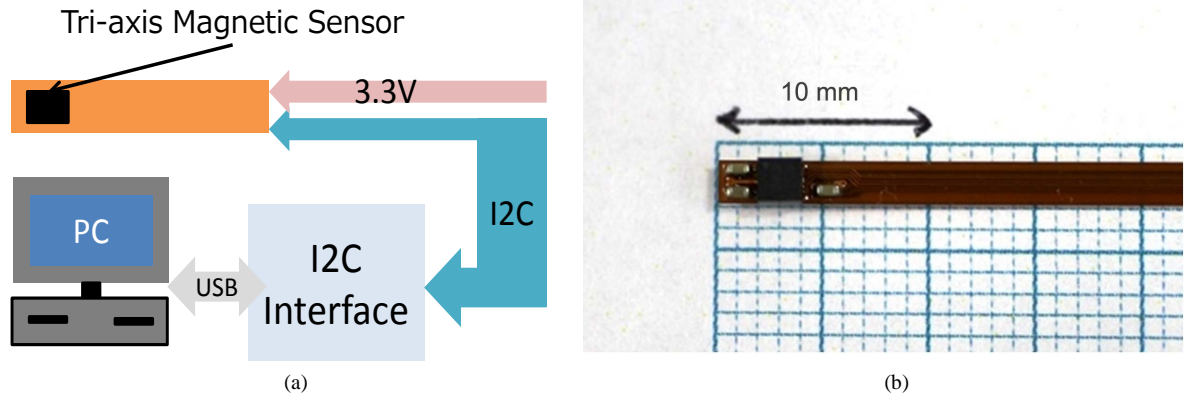**Figure 1.** Schematic diagram of the PEMFC system.

Figure 2. The measurement device of magnetic field in PEMFC. (a) Schematic diagram of the device; (b) Picture of the magneticsensor probe.

$$i_{xn} = \frac{1}{\alpha_x}\left(B_{xn} - B_{x0}\right).$$

$$i_{yn} = \frac{1}{\alpha_y}\left(B_{yn} - B_{y0}\right). \tag{1}$$

where i_{xn} and i_{yn} [A] denote the x and y components, respectively, of the current density at n A; α_x and α_y denote the magnetic field response values for the current; B_{xn} and B_{yn} [G] denote the x and y components, respectively, of the magnetic flux density at n A; and B_{x0} and B_{y0} [G] denote the x and y components, respectively, of the magnetic flux density at 0 A, which are used for removing the effects of geomagnetism and the earth's magnetic field of environment. The current density i_{jn} [A/cm^2] is expressed as follows:

$$i_{jn} = \frac{\sqrt{i_{xn}^2 + i_{yn}^2}}{S}. \tag{2}$$

where S [cm^2] denotes the target area of measurement. However, the sum of i_{jn} for the entire cell may not be equals to the stack current I. Therefore, we revised the expression such that the sum of the current density for the whole cell is equals to the stack current I as follows:

$$i'_{jn} = \frac{\sqrt{i'^2_{xn} + i'^2_{yn}}}{S}. \tag{3}$$

$$i'_{xn} = i_{xn} \times \frac{I}{i}. \quad i'_{yn} = i_{yn} \times \frac{I}{i}. \tag{4}$$

$$i = \sum_{j=1}^{k} i_{jn}. \tag{5}$$

where i'_{yn} [A/cm^2] denotes the revised current density at n A; i'_{xn} and i'_{yn} [A] denote the x and y components, respectively, of the revised current density at n A; and k denotes the number of divisions of the target area for measurement.

The cell area was segmented into 15 parts for calculation, and the measuring points of each cell were set at 15 grid points. Therefore, $k = 15$ in Equation (5). The measured points were $(x, y) = (9, 9)$, $(9, 27)$, $(9, 45)$, $(27, 9)$, $(27, 27)$, $(27, 45)$, $(45, 9)$, $(45, 27)$, $(45, 45)$, $(63, 9)$, $(63, 27)$, $(63, 45)$, $(81, 9)$, $(81, 27)$ and $(81, 45)$. Here, (x, y) denotes position, with units of mm, on the cell surface. The cathode inlet and outlet is located at $(x, y) = (9, 45)$ and $(81, 9)$, respectively.

In order to measure the magnetic fields of cells all at once, the stack was installed in the downward inlet of fuels. The measured cells were cell No. 2, 6, 11, 15, and 20.

3.2. Evaluation Method of a Cell Fault

In order to evaluate the fault such as flooding, measured the z component of the magnetic field and variations in voltage have been used [14].

The z component of magnetic flux density was evaluated to study the three-dimensional current. The z-axis was perpendicular to the surface of the cell. We used the z component of magnetic flux density as an index to explain the current parallel to the surface of the cell. The parallel current is likely arisen the fault such as flooding. The ratio between the value of the z component and the value of the xyz compound vector was calculated at each measurement point. This ratio is defined as follows:

$$B'_z = \frac{B_z^2}{B_x^2 + B_y^2 + B_z^2}. \tag{6}$$

and the parallel current was relatively large when B'_z was large.

The variation in the voltage was useful to identify the cell to arise the flooding. When the cell was flooding, the voltages undergo a change widely because the generated water disturbed the reaction of hydrogen and oxygen. In particular, this trend arises if the flow channel was plug up by the generated water.

4. Results and Discussion

4.1. Stack Performance during Operation

Figure 3 shows the average stack voltage at each air flow rate. The stack voltage decreased as the air flow rate decreased. These air flow rates sufficed the reaction with hydrogen. During these operations, the generated water was steady because the stack current was constant. Furthermore, the experiment started from the 20 L/min. Therefore, the reduction of voltage was attributed to reaction inhibition by the generated water on reactant surface. The cell voltage at 9 and 10 L/min was different however the stack voltage does not appear at Figure 3. The reason was that the stack voltages were average values and the cell voltages undergo a change widely.

4.2. Measurement Results of Magnetic Flux Density

Figure 4 shows vectors of magnetic flux density at 9 L/min. The direction of the vectors was anticlockwise when viewed from the cathode side. This indicates that the direction of the macroscopic current was from the anode side to the cathode side in the stack because of Ampere's law. This direction accorded with the polarity of the stack. In this manner, the macroscopic current in the stack was detected. At cells No. 6, 11, and 15, the values of the z components were smaller than those of the x and y components. In cells No. 2 and 20, the direction of the vectors is different from that in the other cells because they were affected by the end terminals of the stack. Furthermore, in cell No. 2, the values of the z components were larger than those of the x and y components at $(x, y) = (81, 9)$. At the point $(x, y) = (81, 9)$, the current was likely to avoid and flow parallel to the cell surface be-
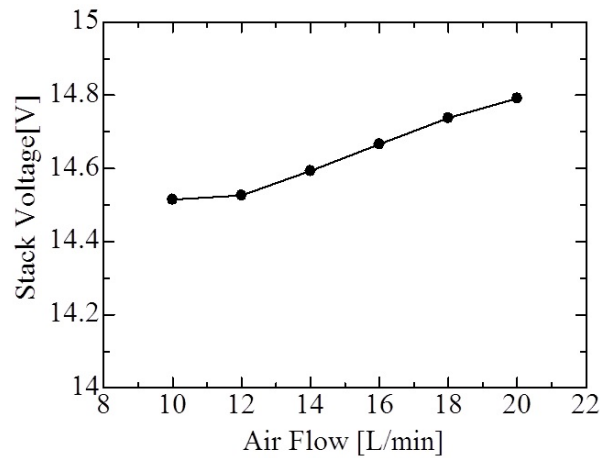
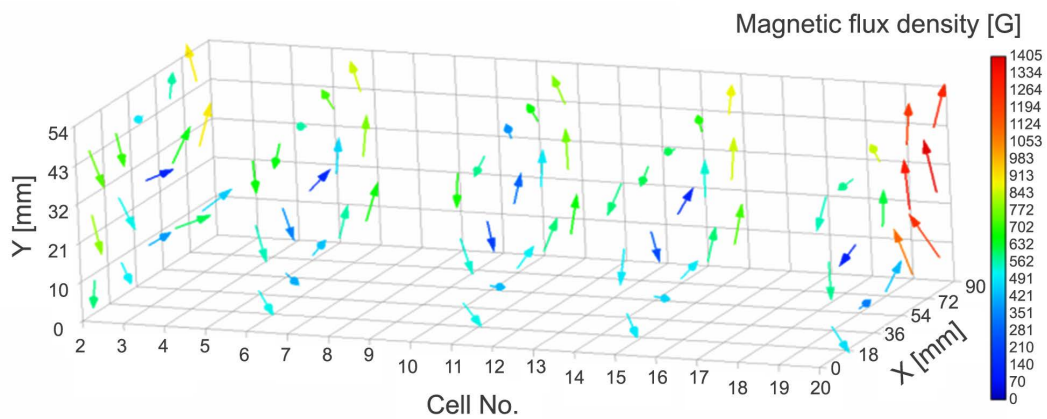**Figure 3.** Stack voltages at each air flow rate.

Figure 4. Magnetic flux density vectors at 9 L/min.

cause of the high electric resistance.

4.3. Current Distribution in Each Cell

Figure 5 shows the current distribution directed toward the z-axis at 20 L/min. The each part of a current was calculated by the Equation (3). The maximum value of current density is 357.5 mA/cm^2 at $(x, y) = (81, 27)$ in cell No. 20. The current distribution tended to be concentrated in the cells at each end of the stack because these cells were affected by the end terminals of the stack. However, current distributions of the cells were not uniform, because each cell exhibited different performance and condition. In the next section, the relationships among the current distributions, the magnetic flux densities, and the cell faults are evaluated.

4.4. Evaluation of Cell Fault

Figure 6 shows the distribution of B'_z on the each cell at 20 L/min. The parallel current increased with increasing B'_z. The cell No. 2 showed the largest B'_z than the other cells. The maximum value of B'_z was 0.75, and this occurred at $(x, y) = (45, 27)$ on the center of cell No. 2. At this point, the current was likely to avoid and flow parallel to the cell surface because of the high electric resistance. Therefore, the current distributions in the center of cells were smaller than those at the other points. The second-highest value of B'_z was 0.31, occurred at $(x, y) = (81, 9)$. At this point, current flow parallel to the cell surface was detected; this was also the case at $(x, y) = (45, 27)$. However, the current distributions were not smaller at these points than at the other points. Therefore, it is considered that the results of the two points are derived from the different phenomena.
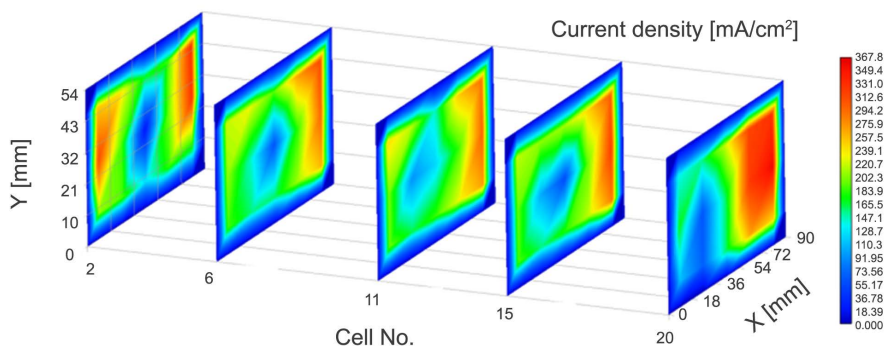
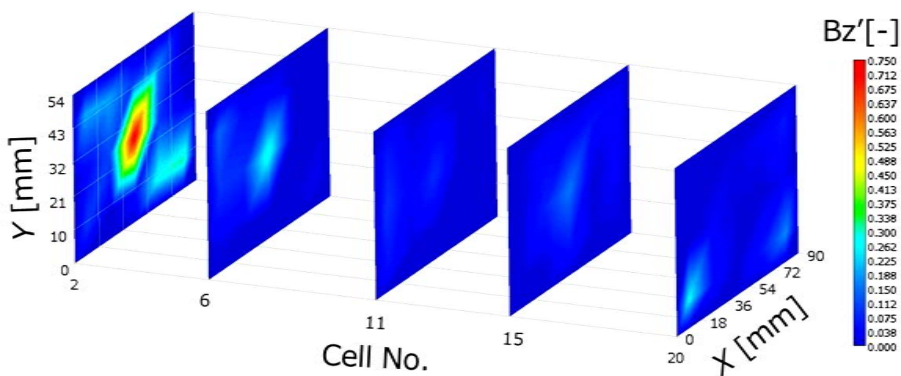**Figure 5.** Current distributions at an air flow rate of 20 L/min.

Figure 6. The distribution of B_z' at 20 L/min.

Figure 7 shows the distribution of B_z' in cell No. 2 each air flow rate. **Figure 8** shows B_z' at the cathode inlet and outlet in cell No. 2 each air flow rate. At the cell center, $(x, y) = (45, 27)$, B_z' decreased with decreasing in the air flow rate. If the flooding occurs in the stack, B_z' increases because of the high electric resistance by the produced water. Therefore, this point did not undergo flooding, and multiple problems of the stack were evaluated. The pressure of membrane might be unequal because the current density was small at this place.

At the cathode inlet, $(x, y) = (9, 45)$, B_z' was almost no variation with the air flow rates. In contrast, B_z' at the cathode outlet, $(x, y) = (81, 9)$ increased with the air flow rate of 9 L/min. The cell voltages varied considerably in cell No. 2, as shown in **Figure 9**. This cell was expected to undergo flooding because the stack was installed in the downward inlet of fuels. Therefore, the point $(x, y) = (81, 9)$ had high electric resistance owing to flooding by the generated water.

5. Conclusions

In this study, the current distribution in a 300-W-class PEMFC stack was investigated using a tri-axis magnetic sensor probe. This measurement device has the advantages of being non-destructive and enabling non-contact measurements.

Through these measurements, we successfully detected the macroscopic current in the stack and observed that the current distribution is concentrated on both ends of the cell because they were affected by the end terminals of the stack.

Furthermore, we evaluated the fault by measuring the z component of the magnetic field, B_z', and variations in the voltage. At the cathode outlet, $(x, y) = (81, 9)$, B_z' was 0.31 when the air flow rate was 20 L/min. At this point, B_z' increased when the air flow rate was 9 L/min. In addition, the cell voltages varied considerably, and cell No. 2 was expected to undergo flooding because the stack was installed in the downward inlet of fuels. Therefore, the point $(x, y) = (81, 9)$ had high resistance due to flooding.

From these results we can conclude that this non-destructive method, using the tri-axis magnetic sensor, can provide significant information about the current distribution and fault occurrences such as flooding in the
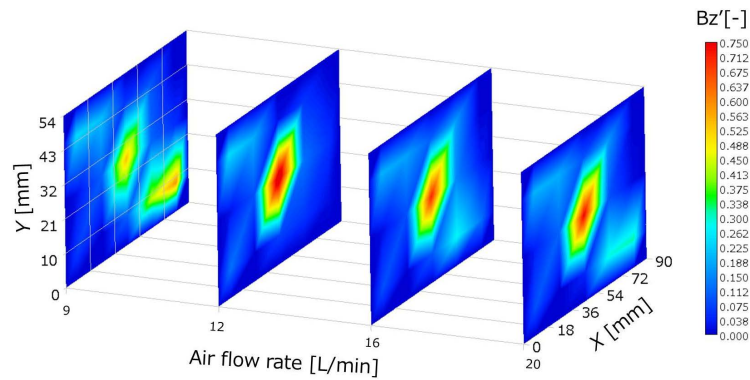
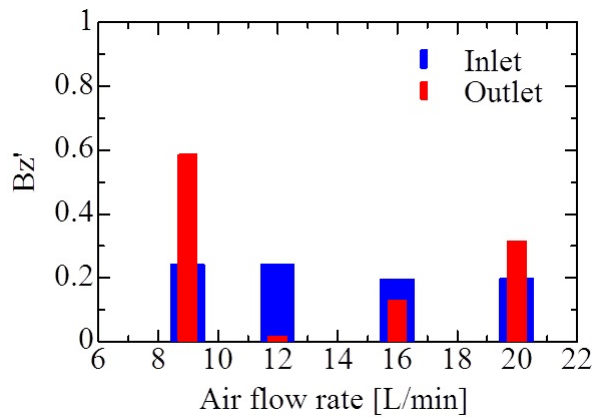**Figure 7.** The distribution of B_z' in cell No. 2.

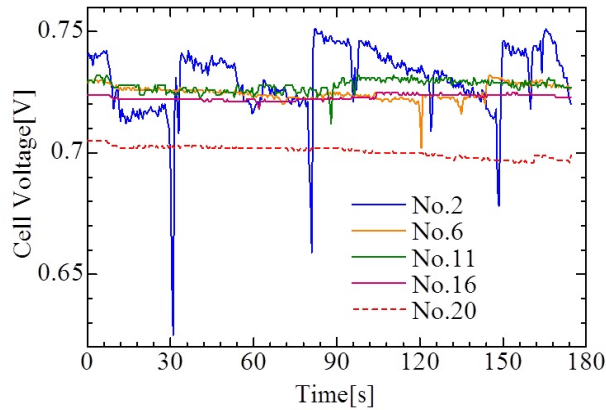**Figure 8.** B_z' at the cathode inlet and outlet in cell No. 2.

Figure 9. Cell voltages at an air flow rate of 9 L/min.

PEMFC. This study has also shown that it is useful to detect the faults by in term as of the *z*-axis magnetic flux density and the cell voltage. This method has shown remarkable potential for the *in-situ* diagnostic applications.

References

[1] Cultura, A.B. and Salameh, Z.M. (2014) Dynamic Analysis of a Stand Alone Operation of PEM Fuel Cell System. *Journal of Power and Energy Engineering*, **2**, 1-8. http://dx.doi.org/10.4236/jpee.2014.21001

[2] Garrain, D., Lechon, Y. and de la Rua, C. (2011) Polymer Electrolyte Membrane Fuel Cells (PEMFC) in Automotive

Applications: Environmental Relevance of the Manufacturing Stage. *Smart Grid and Renewable Energy*, **2**, 68-74. http://dx.doi.org/10.4236/sgre.2011.22009

[3] Wu, J.F., Yuan, X.Z., Martin, J.J., Wang, H.J., Zhang, J.J., Shen, J., Wu, S.H. and Merida, W. (2008) A Review of PEM Fuel Cell Durability: Degradation Mechanisms and Mitigation Strategies. *Journal of Power Sources*, **184**, 104-119. http://dx.doi.org/10.1016/j.jpowsour.2008.06.006

[4] Cleghorn, S.J.C., Derouin, C.R., Wilson, M.S. and Gottesfeld, S. (1998) A Printed Circuit Board Approach to Measuring Current Distribution in a Fuel Cell. *Journal of Applied Electrochemistry*, **28**, 663-672. http://dx.doi.org/10.1023/A:1003206513954

[5] Ghosh, P.C., Wuster, T., Dohle, H., Kimiale, N., Mergel, J. and Stolen, D. (2006) *In-Situ* Approach for Current Distribution Measurement in Fuel Cells. *Journal of Power Sources*, **154**, 184-191. http://dx.doi.org/10.1016/j.jpowsour.2005.03.219

[6] Wieser, Ch., Helmbold, A. and Gue Lzow, E. (2000) A New Technique for Two-Dimensional Current Distribution Measurements in Electrochemical Cells. *Journal of Applied Electrochemistry*, **30**, 803-807. http://dx.doi.org/10.1023/A:1004047412066

[7] Alaefour, I., Karimi, G., Jiao, K., Al Shakhshir, S. and Li, X. (2011) Experimental Study on the Effect of Reactant Flow Arrangements on the Current Distribution in Proton Exchange Membrane Fuel Cells. *Electrochimica Acta*, **56**, 2591-2598. http://dx.doi.org/10.1016/j.electacta.2010.11.002

[8] Alaefour, I., Karimi, G., Jiao, K. and Li, X. (2011) Measurement of Current Distribution in a Proton Exchange Membrane Fuel Cell with Various Flow Arrangements—A Parametric Study. *Applied Energy*, **93**, 80-89. http://dx.doi.org/10.1016/j.apenergy.2011.05.033

[9] Sasabe, T., Tsushima, S. and Hirai, S. (2010) *In-Situ* Visualization of Liquid Water in an Operating PEMFC by Soft X-Ray Radiography. *International Journal of Hydrogen Energy*, **35**, 11119-11128. http://dx.doi.org/10.1016/j.ijhydene.2010.06.050

[10] Tsushima, S., Teranishi, K. and Hirai, S. (2005) Water Diffusion Measurement in Fuel-Cell SPE Membrane by NMR. *Energy*, **20**, 235-245. http://dx.doi.org/10.1016/j.energy.2004.04.013

[11] Hauer, K.-H., Potthast, R., Wüster, T. and Stolten, D. (2005) Magnetotomography—A New Method for Analyzing Fuel Cell Performance and Quality. *Journal of Power Sources*, **143**, 67-74. http://dx.doi.org/10.1016/j.jpowsour.2004.11.054

[12] Izumi, M., Gotoh, Y. and Yamanaka, T. (2009) Verification of Measurement Method of Current Distribution in Polymer Electrolyte Fuel Cells. *ESC transactions*, **17**, 20401-20409.

[13] Katou, T., Gotoh, Y., Takahashi, N. and Izumi, M. (2012) Measurement Technique of Distribution of Power Generation Current Using Static Magnetic Field around Polymer Electrolyte Fuel Cell by 3D Inverse Problem FEM. *Materials Transactions*, **53**, 279-284.

[14] Nasu, T., Matsushita, Y., Okano, J. and Okajima, K. (2012) Study of Current Distribution in PEMFC Stack Using Magnetic Sensor Probe. *Journal of international Council on Electrical Engineering*, **2**, 391-396. http://dx.doi.org/10.5370/JICEE.2012.2.4.391

[15] Okajima, K., Nasu, T. and Choi, S. (2014) Evaluation of 1-kW Class PEM Fuel Cell Stack under *In-Situ* Conditions Considering Individual Cells. *Journal of Energy and Power Engineering*, **8**, 1543-1551.